J Inorg Organomet Polym (2013) 23:1296–1304
DOI 10.1007/s10904-013-9922-x

Structure and Spectral Properties of Pyrazine Ligand Assisted Self-Assembly of a Coordination Polymer Containing Copper-Cyanide Building Blocks

Safaa Eldin H. Etaiw · Safaa N. Abdou

Received: 21 April 2013 / Accepted: 29 July 2013 / Published online: 11 August 2013

Abstract The metal–organic framework $^{3}_{\infty}[Cu_3(CN)_3\cdot(pyz)_2]$, **1,** (*pyz* pyrazine) was prepared in water/acetonitrile solvent at ambient temperature from the adducts $K_3[Cu(CN)_4]$, pyrazine and Me_2SnCl_2. The structure of **1** consists of four-coordinate Cu(1) sites exhibiting a distorted tetrahedral geometry and the linear two-coordinate Cu(2) sites. Notably distorted cages, $[Cu_8(CN)_4(pyz)_4]$, $[Cu_8(CN)_6(pyz)_2]$ and $[Cu_6(CN)_2(pyz)_4]$, can be considered as the basic building blocks of the structure of **1**. Box-like structures create inextricably interpenetrated equivalent 3D-frameworks. The structure and spectroscopic properties of **1** were also investigated by thermal analysis and IR, mass, UV/Vis and fluorescence spectra.

Keywords Metal–organic framework · Copper cyanide · Pyrazine · Spectra

1 Introduction

The metal–organic frameworks (MOF) containing copper(I) cyanide have become the focus of interest because of the large number of these compounds with a remarkable diversity of structures [1–4] and a large range of potential applications as composite inorganic–organic zeolitic materials [5–7], catalysts [3, 8–10], precursor in the synthesis of ceramic superconductors [11], cyanocuprate reagent in synthetic organic chemistry [12], and antitumor agents [8, 13, 14]. Beside the curiosity in the construction of frameworks with copper(I)-cyanide as design elements, an interest in the special luminescent properties of copper(I)-cyanide complexes have driven researchers to explore this system. The small cyanide group has a rigid linear structure with an extended conjugated π-electron system possessing good potential ability to enhance photoelectron transfer and non-linear optical reactivity. Recent studies reveal that copper(I)-cyanide complexes can exhibit particular luminescent properties with abundant optical transitions [15–18]. The copper(I)-cyanide system is also attractive from the point of view of crystal engineering. The cyanide group is capable of functioning as a straight connector to yield a linear –Cu–CN– chain in copper(I)-cyanide. Copper(I) ion favors trigonal or tetrahedral coordination in the presence of cyanide and the dipodal groups. These groups offer the possibility of promoting the formation of frameworks because of the strong coordinating nature of these ligands and their ability to act as connector between different copper centers [17, 19, 20].

There are different synthetic strategies of preparing copper(I)-cyanide coordination polymers [12, 21]. In the course of our investigation of bimetal-organic frameworks [13, 22, 23], we intended to synthesize a bimetallic coordination polymer containing the $(Me_2Sn)^{2+}$ cation, $(CuCN)_n$ fragment and pyrazine ligand at ambient temperature. However, $^{3}_{\infty}[Cu_3(CN)_3\cdot(pyz)_2]$ (**1**) was obtained. Herein, we report the synthesis, crystal structure, thermal stability as well as spectral and fluorescent properties of **1**.

2 Experimental

All reagents were purchased from Aldrich and Sigma and were used as received. $K_3[Cu(CN)_4]$ was prepared following the literature procedure [3]. Microanalyses (C, H

S. E. H. Etaiw (✉)
Chemistry Department, Faculty of Science,
Tanta University, Tanta, Egypt
e-mail: safaaetaiw@hotmail.com

S. N. Abdou
Chemistry Department, Faculty of Education and Science
(Khourma), Taif University, Taif, Saudi Arabia

and N) were carried out with a Perkin Elmer 2400 automatic elemental analyzer. The IR spectra were recorded on a Bruker Vector 22 spectrophotometer as KBr disks. Mass spectra were recorded on a Finnigan MAT 8222 by FAB spectrometer. Thermogravimetric analysis was carried out on a Shimadzu AT 50 thermal analyzer under a N_2 atmosphere. Electronic absorption spectra were measured as Nujol mull matrices on a Shimadzu (UV-310PC) spectrometer. Luminescence spectra as solid matrices were recorded at an excitation wavelength 280 nm using a Perkin Elmer (LS 50 B) spectrometer.

2.1 Synthesis of $^{3}_{\infty}[Cu_3(CN)_3\cdot(pyz)_2]$, **1**

A solution of $K_3[Cu(CN)_4]$ (44 mg, 0.155 mmol) in H_2O (10 ml) was added with gentle stirring to a mixture of hot solutions containing Me_2SnCl_2 (100 mg, 0.47 mmol) in acetonitrile (10 ml) and pyrazine (12 mg, 0.155 mmol, pyz) in acetonitrile (10 ml). After 10 days, orange needle crystals grew from an initially clear solution. After filtration, washing with small quantities of warm H_2O and acetonitrile and overnight drying, orange needle crystals (32 mg, 48.5 % based on $K_3[Cu(CN)_4]$) were obtained. All attempts to synthesize **1** in the absence of Me_2SnCl_2 were unsuccessful under identical experimental conditions. Anal. Calc. (%) for **1** ($C_{11}H_8N_7Cu_3$): C, 30.79; H, 1.86; N, 22.86; Cu, 44.47. Found: C, 30.65; H, 1.92; N, 22.73; Cu, 44.10.

2.2 X-Ray Structural Determination of **1**

Structural measurements for **1** were performed on a Kappa CCd EnrafNonius FR 590 four-cycle goniometer with graphite monochromatic MoK_∞ radiation source {$\lambda = 0.71073$ Å} at 25 °C. The structure was resolved using direct methods and all the non-hydrogen atoms were located from the initial solution or from subsequent electron density difference maps during the initial stages of the refinement. After locating all of the non-hydrogen atoms in each structure the models were refined against F2, first using isotropic and finally using anisotropic thermal displacement parameters. The positions of the H-atoms were then calculated and refined isotropically. Then the final cycle of refinements was performed. Crystallographic data for **1** are summarized in Table 1. Selected bond distances and bond angles are given in Table 2.

Table 1 Crystal data and structure refinement parameters of **1**

Empirical formula	$C_{11}H_8N_7Cu_3$
Formula weight (g mol^{-1})	428.872
Temperature (K)	298
Wavelength (Å)	0.71073
Crystal system	Monoclinic
Space group	C 2/m
Unit cell dimensions	
a (Å)	12.3635(11)
b (Å)	10.3210(8)
c (Å)	5.6531(3)
α (°)	90.00
β (°)	93.849(2)
γ (°)	90.00
V ($Å^3$); Z	719.73(9)/2
ρ calc. (mg m^{-3})	1.979
Absorption coefficient (mm^{-1})	4.39
F (000)	420
Reflections collected/unique	4617/654
R int	0.032
Data/restraints/parameters	654/0/56
Goodness-of-fit on F^2	2.242
R indices [I > 3 σ (I)] R^1/wR^2	0.060/0.158
W = 1/s^2^ (Fo^2^) + 0.10000× Fo^2^)	
R indices (all data)	0.077/0.159
Largest difference peak and hole	1.69/−0.75 e $Å^{-3}$

Table 2 Selected bond lengths (Å) and bond angles (°) for **1**

Cu(1)–N(3)	2.123(3)	Cu(1)–N(4)–C(8)	178.1(4)
Cu(1)–N(4)	1.925(5)	N(3)–Cu(1)–N(3)	97.33(14)
Cu(1)–X(5)	1.920(5)	N(3)–Cu(1)–N(4)	103.58(11)
Cu(2)–C(8)	1.854(6)	N(3)–Cu(1)–X(5)	110.60(10)
N(4)–C(8)	1.149(8)	N(4)–Cu(1)–X(5)	127.0(2)
X(5)–X′(5)	1.151(9)	C(8)–Cu(2)–C(8)	180.0000
Cu(1)–X(5)–X′(5)	176.4(5)	Cu(2)–C(8)–N(4)	175.0(5)

3 Results and Discussion

3.1 X-Ray Diffraction of Single Crystal and Structure of **1**

The 3D-coordination polymer, **1**, $^{3}_{\infty}[Cu_3(CN)_3\cdot(pyz)_2] \equiv^{3}_{\infty}[(CuCN)_2(\mu{-}(CuCN)(\mu\text{ - }pyz)_2]$, crystallizes in the monoclinic space group C2/m with unit cell dimensions a = 12.3635 Å (11), b = 10.3210 Å (8), c = 5.6531 Å (3), β = 93.849° (2), Z = 2. Figures 1 and 2 shows the ORTEP plot of the asymmetric unit of **1** and the extended structure with the atom labeling scheme. The asymmetric unit of **1** is surprising simple (Fig. 1) consisting of Cu(1) with identity symmetry operation, Cu(2) exhibiting inversion center at [0,0,0], one ordered and one disordered cyanide groups (C(5) with twofold rotation axis) and half a pyz molecule [N(3),C(6) and C(7)], which exhibits an inversion center at [1/4,1/4,0] and mirror and glide planes, respectively. On the other hand, the extended structure of **1** involves not only two crystallography different Cu(1) and Cu(2) sites and three cyanide groups, but also the bipodal

pyz ligand. Each Cu(1) site is four-coordinate to two pyz rings, one ordered cyanide group and one disordered cyanide group. Thus, Cu(I) site has a distorted tetrahedral geometry, which is a characteristic feature of copper(I) [24]. This is also indicated by the bond angles; N_4–Cu_1–$X_5 = 127.0°$, N_3–Cu_1–$X_5 = 110.60°$, N_3–Cu_1–$N_3 = 97.33°$ and N_3–Cu_1–$N_4 = 103.58°$, (Table 2). The structure of **1** involves also the classical two-coordinate copper(I) site, Cu(2), which is linked by two ordered cyanide groups. This particular coordination is known in the solid state where polymeric units are built with linear coordination of copper(I) atoms in cuprous oxide [24], cuprous chromite [25], [Cu X_2] [26], Cu C_2 [27], Cu N_2 [28] and Cu S_2 [29]. Thus, the structure of **1** may be described as infinite, but nonlinear, $\{Cu(1)pyz\}_\infty$ and –[–Cu(1)–C(5)N(5)–Cu(1)–C(4)N(8)–Cu(2)–N(8)C(4)] chains that cross each other at the quasi-tetrahedral Cu(1) sites thereby creating a 3D framework.

The $(Cu(1)CN)_2$ fragments represent the main building blocks, which are connected in a unique way by Cu(2)CN as bridging units to form non-linear chains. The Cu_1–C–N angles exhibit a deviation from linearity (Table 2) while the spacer N–C–Cu_2–C–N adopts linear geometry with an angle of 180°. The CuCN chains construct layers with wide channels occupied by two crossing sets of pyz rings, which form with CuCN chains into interpenetrating 3D-layered structures (Figs. 3 and 4). The distance between pyz-linked Cu_1 sites is 6.9 Å. The crossing of the Cu-pyz-Cu zig-zag chains cause diamondiod voids connected by the cyanide group (Fig. 3). The network structure of **1** involves 3D Cu(1) sites with two nearly perpendicular pyz rings. The N_3–Cu_1–N_3 angle is 97.33° forming a stair construction (Fig. 4). The Cu-pyz-CuCN fragment forms parallel zig-zag chains connected to another neighboring interpenetrating Cu-pyz-Cu–CN fragment, which is connected by the CN–Cu_2–CN spacer to form a parallel 3D-layered structure that contains fused distorted hexagonal rings. The $Cu_8(CN)_6(pyz)_2$ ring displays edges that exhibit different lengths; (Cu–pyz–Cu, 7.052 Å); (Cu–CN–Cu–CN–Cu, 9.842 Å) and (Cu–CN–Cu, 4,99 Å) (Fig. 5). These parallel layers are connected by the nearly perpendicular pyz rings creating two types of interpenetrating distorted hexagonal rings, $Cu_6(CN)_2(pyz)_4$ and $Cu_8(CN)_6(pyz)_2$ (Figs. 6 and 7). The first ring contains Cu(1)-atoms while the second contains both Cu(1)- and Cu(2)-atoms. The two rings share each other with Cu_1-pyz-Cu_1 sides. These rings form box-like structures and are considered the main cause of producing inextricably interpenetrating equivalent networks (Fig. 8).

The network structure was further stabilized by π–π stacking of the pyz rings, which is supported by the distance 3.1893 Å between the neighboring pyz rings and by extensive H-bonding. The H-bonds are formed between the H-atoms of pyz and the donor sites of the $(CuCN)_n$ fragment (2.75–3.06 Å) and between the H-atoms in one pyz ring and the π–cloud of the other faced pyz ring. These unconventional H-bonds exhibit relatively long distances in the range of 3.13–3.36 Å. In addition to the previous two forces causing stabilization of the network structure of **1**, one could not ignore the Van der Waals forces, which play an important role in stabilizing the network structure of **1**,

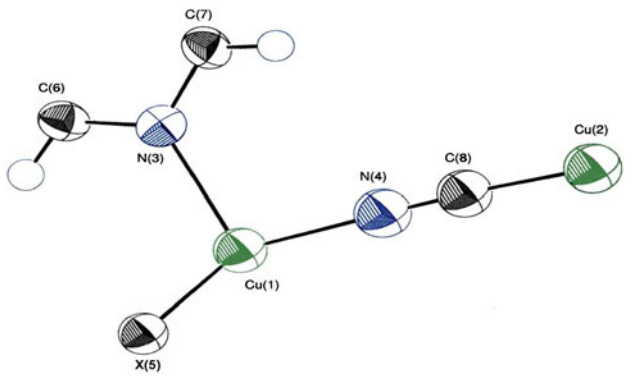

Fig. 1 ORTEP drawing of the asymmetric unit of **1**, showing the atom labeling scheme. (Thermal ellipsoids are shown 50 % probability)

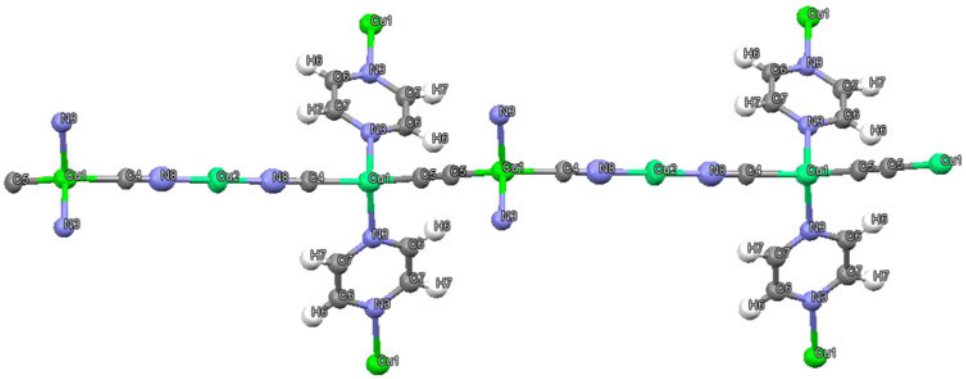

Fig. 2 The extended structure of **1**, along the c-axis showing the atom labeling scheme

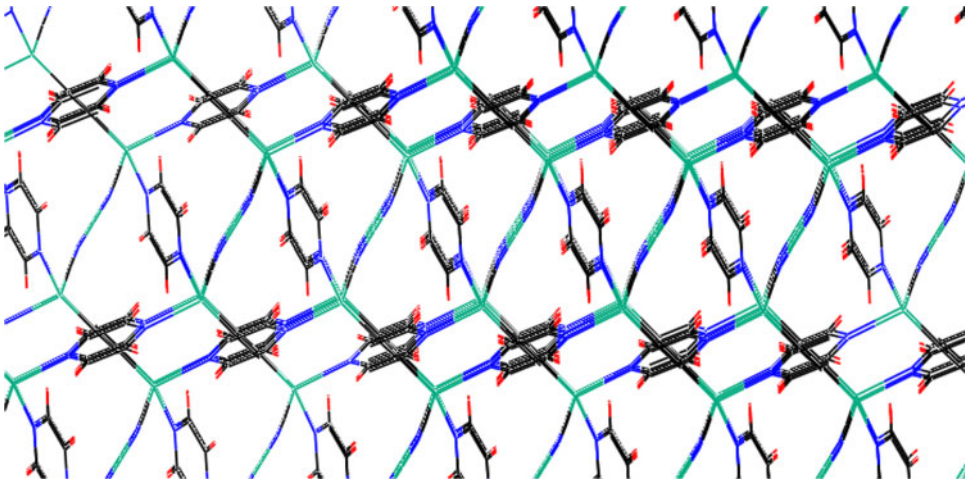

Fig. 3 A view of the 3D-layer structure of **1** along the a-axis showing the distorted fused hexagonal rings

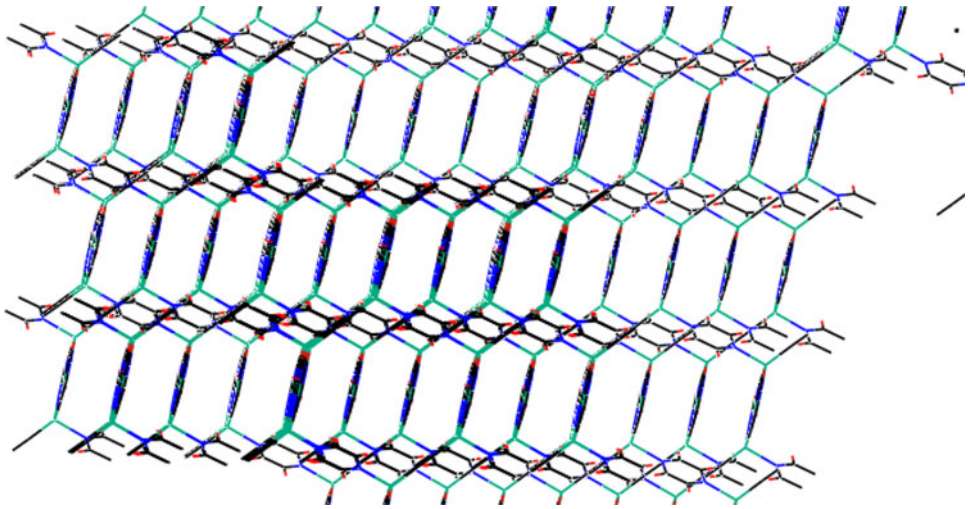

Fig. 4 A view of the network structure of **1** showing the stair construction along the c-axis

between pyz rings exhibiting intermolecular distances in the range of 3.45–3.62 Å.

3.2 Infrared Spectrum of 1

The IR spectrum of **1** exhibits bands characteristics of the $(CuCN)_n$ fragment and the bipodal ligand, pyz, (Tables 3 and 4). The bands for pyz are almost identical to those found in **1**. The bands at 3076, 3030, 1411, 793 and 698 cm^{-1} corresponding to ν_{CH}, δ_{CH} and γ_{CH} of pyz, respectively; they shift to lower wavenumbers due to the formation of hydrogen bonds between the H-atoms of pyz and the doner sites of the $(CuCN)_n$ fragment [30]. On the other hand, the bands at 1478, 1520, 1543 cm^{-1} and at 1605 cm^{-1} due to $\nu_{C=C}$ and $\nu_{C=N}$ of pyz exhibit small shifts to lower wavenumbers than those of pyz itself thereby supporting the formation of hydrogen bonds and pyz coordination to the Cu(I) sites. The IR spectrum of **1** shows strong bands due to skeletal and C–C vibrations of pyz at 1162, 1121, 1074, 1044 and 439 cm^{-1}. Moreover, the $(CuCN)_n$ fragment absorbs at wavenumbers in the normal range of $\nu_{C\equiv N}$; i.e., 2151, 2122 and 2104 cm^{-1}. It is worth mentioning that the $\nu_{C\equiv N}$ bands of **1** are different than those of $K_3[Cu(CN)_4]$, which is potentially used as one of the adducts for the formation of **1**; however, they are similar to those of CuCN. The $\nu_{C\equiv N}$ bands of $K_3[Cu(CN)_4]$ appear below 2100 cm^{-1}; i.e., at 2081, 2075, 2040, 2032 cm^{-1}; and, a weak band at 2170 cm^{-1} is characteristic of the tetrahedrally configured $[Cu(CN)_4]^{-3}$. The structure of **1** is quite different than that of $K_3[Cu(CN)_4]$; however, it contains the $(CuCN)_n$ fragment and the tetrahedral Cu(I) sites. The presence of the $\nu_{C\equiv N}$ bands in **1** supports the presence of two different cyanide groups; one is disordered and one is ordered. The stretching vibrations of the Cu–C bond appear as a weak band at 408 cm^{-1}. Thus, the IR spectrum of **1** supports the presence of the $(CuCN)_n$ fragment and the bipodal pyz ligand, which is coordinated to the tetrahedral Cu(I) sites.

3.3 Mass Spectrum of 1

The constitution and purity of **1** are established by mass spectrometry (Table 5). The mass spectrum of **1** shows two

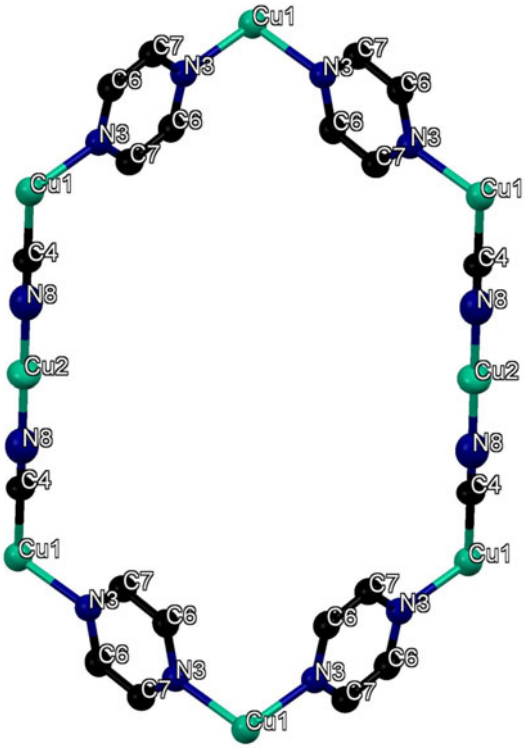

Fig. 5 A view of the hexagonal ring $[Cu_8(CN)_4(pyz)_4]$ of **1** along the b-axis showing the orientation of the pyz ligands. Hydrogen atoms are omitted for clarity

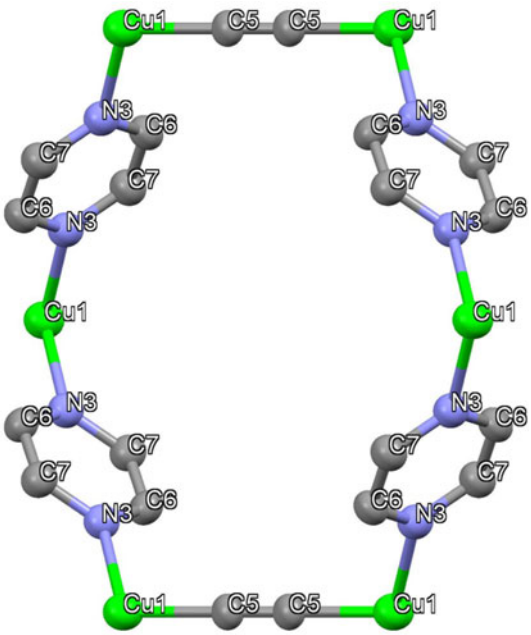

Fig. 6 A view of the distorted hexagonal ring $[Cu_6(CN)_2(pyz)_4]$ of **1** along the b-axis showing the orientation of the pyz ligands. Hydrogen atoms are omitted for clarity

ion peaks for the pyz fragment at m/z 52 due to $[C_4H_4]^+$ and m/z 80 corresponding to $[pyz]^+$. The mass spectrum also exhibits m/z 91, 143, 152, 162, 173 and 223, which correspond to $[CuCN]^+$, $[Cu\text{-}pyz]^+$, $[Cu_2CN]^+$, $[2(pyz)]^+$, $[CuCN(pyz)]^+$ and $[Cu\text{-}pyz\text{-}Cu]^+$, respectively. The ion peaks at m/z 236, 244, 316, 322, 342 and 401 are due to $[Cu_2CN(pyz)]^+$, $[Cu_3(CN)_2]^+$, $[Cu_2CN(pyz)_2]^+$, $[Cu_3(CN)_2(pyz)]^+$, $[Cu_2(CN)_2(pyz)_2]^+$ and $[Cu_3(CN)_2(pyz)_2]^+$, respectively. Additional peaks at m/z 432 and 854 corresponding to $[Cu_3(CN)_3(pyz)_2]^+$ and corresponds to the molecular weight of **1** and $[Cu_6(CN)_6(pyz)_4]^+$, respectively. In addition, the mass spectrum displays peaks from m/z 499 to 1006, which correspond to $[Cu_3(CN)_3(pyz)Cu_2CN]^+$ and $[Cu_3(CN)_3(pyz)_2Cu_3(CN)_3(pyz)_2Cu_2CN]^+$, respectively, thus supporting the polymeric nature of the $Cu_3(CN)_3$ building blocks. Thus, the mass spectrum of **1** confirms the presence of polymeric CuCN fragments connected by the bipodal pyz ligand.

3.4 Thermogravimetric Analysis of 1

The thermal analysis of $[Cu_3(CN)_3{\cdot}(pyz)_2]$, **1** takes place in four steps (Table 6). The first step occurs from 100 to 200 °C and corresponds to the release of the two pyrazine molecules [obs. $\Delta m = -37.14$ %, 159.20 g mol^{-1}; calcd. $\Delta m = -37.32$ %, 160 g mol^{-1}]. This step is followed by the release of the cyanide group from 210 to 300 °C [obs. $\Delta m = -5.88$ %, 25.24 g mol^{-1}; calcd. $\Delta m = -6.06$ %, 26 g mol^{-1}]. The third step from 310 to 440 °C, corresponds to the release of two cyanide groups [obs. $\Delta m = -12.23$ %, 52.42 g mol^{-1}; calcd. $\Delta m = -12.13$ %, 52 g mol^{-1}]. This step is followed by a small increase in the mass due to the gain of oxygen from 460 to 490 °C [obs. $\Delta m = +3.62$ %, 15.53 g mol^{-1}; calcd. $\Delta m = +3.73$ %; 16 g mol^{-1}]. At higher temperatures over 500 °C, **1** oxidizes leading to the final product of cuprous oxide and copper. The molecular weight of the residue obtained after complete thermolysis of **1** is coincident with $Cu + Cu_2O$ [obs. m = 48.37 %, 207.33 g mol^{-1}); calcd. m = 48.18 %, 206.55 g mol^{-1}]. Thus, the thermogravimetric data indicate that **1** contains the CuCN fragment and the bipodal pyz ligand.

3.5 Electronic Absorption and Emission Spectra of pyz and 1

The electronic absorption spectra of pyrazine and **1** reveal absorption bands at 230–300 nm. The spectrum of pyz displays two absorption bands at 255 and 295 nm. The first band corresponds to $^1L_b \leftarrow {}^1A$ transition. This band substantiates the assignment made for pyridine (252 nm) and pyrazine (260 nm) [31]. The second band at 295 nm exhibits a weak intensity and disappears on addition of HCl indicating an n–π^* transition. The first absorption band in **1** at 230 nm is not observed for pyrazine and is attributed to a metal–ligand charge transfer. The second band at 255 nm

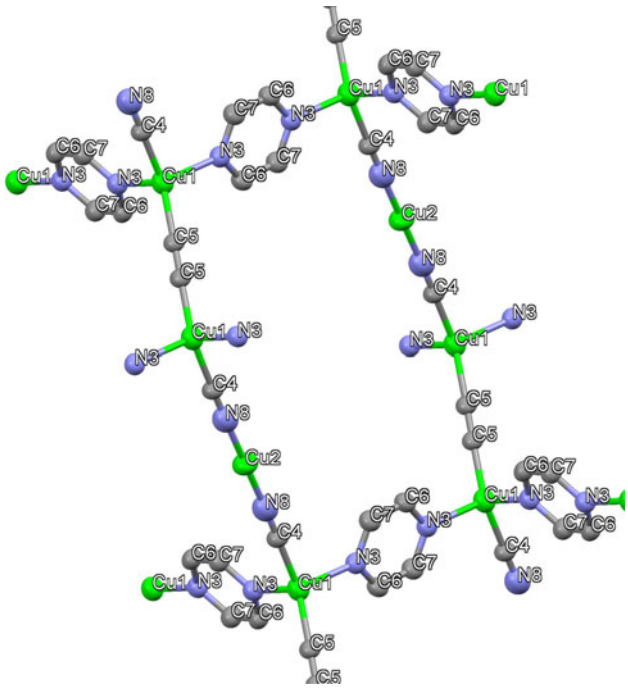

Fig. 7 A view of the distorted hexagonal ring [Cu8(CN)6(pyz)2] of **1** along the a-axis showing the orientation of the pyz ligands. Hydrogen atoms are omitted for clarity

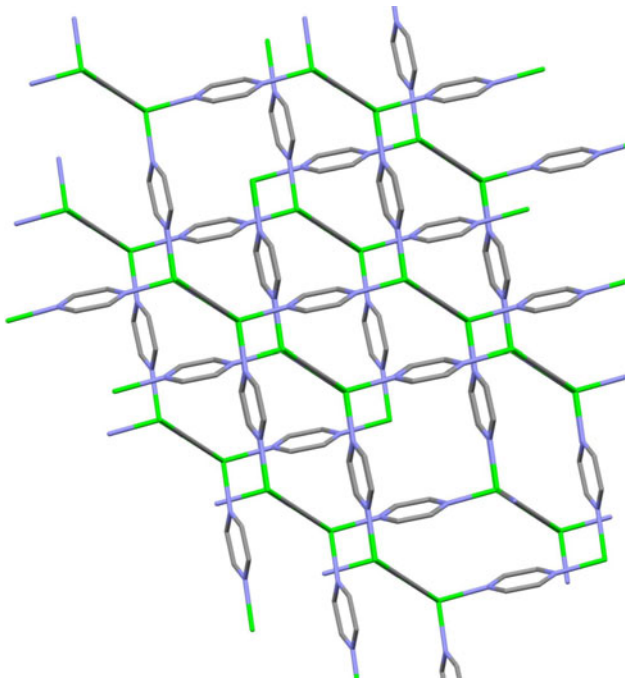

Fig. 8 A view of the inextricably interpenetrated equivalent networks of **1**. Hydrogen atoms are omitted for clarity

Table 3 Wavenumbers (cm^{-1}) of the different vibrational modes of pyz

Peak	Assignment	Peak	Assignment	Peak	Assignment
3090 m	ν_{CH}	1540m	$\nu_{C=C}$	1170 m	Skeletal and C–C vibs. (pyz)
3040 w		1482m		1149 s	
				1098 m	
				1064 s	
				1026 m	
1610 w	$\nu_{C=N}$	1414 s	δ_{CH}	795 s	γ_{CH}

Table 4 Wavenumbers (cm^{-1}) of the different vibrational modes of **1**

Peak	Assignment	Peak	Assignment	Peak	Assignment
3076 w	ν_{CH} (pyz)	1520 w	$\nu_{C=C}$ (pyz)	793 s	γ_{CH} (pyz)
3030 w		1478 m			
2150 m	$\nu_{C\equiv N}$	1410 s	δ_{CH} (pyz)	408w	ν_{Cu-C}
2122 s					
2104 s					
1605 m	$\nu_{C=N}$(pyz)	1162 s	Skeletal and C–C vibs. (pyz)		
		1121 s			
		1074 m			
		1044 s			
		1010 w			

s strong; *m* medium; *w* weak

Table 5 Interpretation of the mass spectrum of **1**

Ion	M/z	Ion	M/z
$[C_4H_4]^+$	52	$[Cu_3(CN)_2(pyz)_2]^+$	401
$[pyz]^+$	80	$[Cu_3(CN)_3(pyz)_2]^+ \equiv$ {M.W}	432
$[CuCN]^+$	91	$[Cu_3(CN)_3(pyz)Cu_2CN]^+$	499
$[Cu\text{-}pyz]^+$	143	$[Cu_3(CN)_3(pyz)_2CuCN]^+$	517
$[Cu_2CN]^+$	152	$[Cu_3(CN)_3(pyz)_2Cu(pyz)]^+$	576
$[2(pyz)]^+$	162	$[Cu_3(CN)_3(pyz)_2Cu(pyz)_2]^+$	650
$[CuCN(pyz)]^+$	173	$[Cu_3(CN)_3(pyz)_2Cu_3(CN)_3]^+$	698
$[Cu\text{-}pyz\text{-}Cu]^+$	223	$[Cu_3(CN)_3(pyz)_2Cu_2CN(pyz)_2]^+$	739
$[Cu_2CN(pyz)]^+$	236	$[Cu_3(CN)_3(pyz)_2Cu_2(CN)_2(pyz)_2]^+$	766
$[Cu_3(CN)_2]^+$	244	$[Cu_3(CN)_3(pyz)_2Cu_3(CN)_3(pyz)]^+$	776
$[Cu_2CN(pyz)_2]^+$	316	$[Cu_6(CN)_6(pyz)_4]^+ \equiv 2${M.W}	854
$[Cu_3(CN)_2(pyz)]^+$	322	$[Cu_6(CN)_6(pyz)_4Cu_2CN]^+$	1006
$[Cu_2(CN)_2(pyz)_2]^+$	342	–	–

resembles that observed for pyz, which corresponds to the $^1L_b \leftarrow {}^1A$ transitions. The long wavelength band at 300 nm is assigned to a π–π* transitions of the cyanide group. The disappearance of the band due to *n*–π* transition supports the coordination of copper atoms to the nitrogen atoms of pyz. On the other hand, the solid

Table 6 Thermogravimetric analysis data of **1**

Temp. range °C	Δm_{obs} % mass unit (M.W.) g mol^{-1}	Δm_{cal} % mass unit (M.W.) g mol^{-1}	Steps
100–200	−37.14 % (159.2)	−37.32 % (160)	−[2 (pyz)]
210–300	−5.88 % (25.24)	−6.06 % (26)	−(CN)
310–440	−12.23 % (52.42)	−12.13 % (52)	−2(CN)
460–490	+3.62 % (15.53)	+3.73 % (16)	+(O)
Over 500	48.37 % (207.33)	48.18 % (206.55)	Cu + Cu_2O

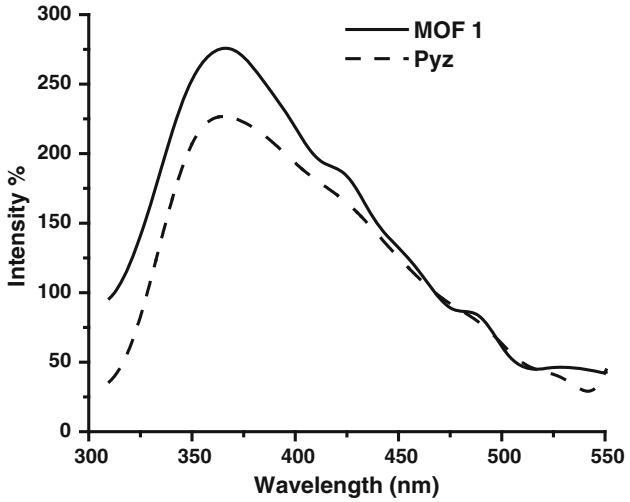

Fig. 9 Emission spectra (λ_{ex} = 280 nm) of pyz and **1** in solid state

matrices of pyrazine and **1** exhibit a strong luminescence. Pyrazine luminesces at 355 nm while **1** exhibits an emission bands at 360 nm, which resembles pyz, and at 430 nm (Fig. 9). It is well known that CuCN luminesces at 390 nm while the amine-bearing CuCN complexes emits in the visible region. Nevertheless, the photo-physical behavior of the CuCN-amine networks appears to be closely related to CuCN itself [32, 33]. Thus, the emission band at 430 nm of **1** resembles that of CuCN [20] which is assumed to arise from transitions from the lowest excited-triplet state to the ground state. Lifetime studies of soluble Cu(1)-cyano species have suggested that emission is usually a phosphorescence phenomenon [15, 34]. The red shift and the relatively high intensity of the emission bands of **1** relative to CuCN may be due to three-coordinate copper centers and the bent structure of the CuCN chains, which allow for the distortion that is obtained in the bent triplet structures that produce multiple triplet states [35].

3.6 Synthesis and Further Discussion

The reaction of $K_3[Cu(CN)_4]$ with Me_2SnCl_2 and pyz in water/acetonitrile affords the orange needle crystals $^{3}_{\infty}[Cu_3(CN)_3\cdot(pyz)_2] \equiv ^{3}_{\infty}\left[(CuCN)_2(\mu\text{ - }CuCN)(\mu\text{ - }pyz)_2\right]$, **1**. The structure of the organotin–free product seems to be quite different from earlier reported bi-heterometallic product of [CuCN - Me_3SnCN - pyz] $\equiv ^{3}_{\infty}$ [Cu(μ - pyz) (μ - CN Sn (Me_3)NC], **2**, which was prepared in the presence of Me_3SnCl instead of Me_2SnCl_2 [36]. On the other hand, **1** was obtained in a mixture containing lamellar yellow crystals of $^{2}_{\infty}\left[Cu_3(CN)_3(pyz)\right]$, **3**, from the hydrothermal reaction of CuCN, KCN, pyz and H_2O in a 23 ml Parr acid digestion vessel heated at 180 ± 5 °C for 125 h [37]. Attempts to prepare monophasic samples of **1** and **3** under hydrothermal conditions proved unsuccessful. Thus, different routes have turned out to be useful for the generation of single crystals of $[(Cu_n(CN)_m\cdot xL]$ and $[(Cu)_n\ (CN)_m\ (R_3Sn)_y\ xL]$ suitable for X-ray crystallography. The first strongly resembles the method of preparation of **1** and **2** [18, 36] in that an aqueous solution of either authentic or in situ-prepared $K_3[Cu(CN)_4]$ is added to a solution of the bipodal organic ligand L and the organotin compound in water/acetonitrile solution. The products should be either the organotin-free or the organotin-containing species. The second route makes use of the very slow transfer of Me_3SnCl molecules from the gas phase above a sample of solid Me_3SnCl (or of a concentrated aqueous solution) into an aqueous solution of $K_3[Cu(CN)_4]$, the dipodal ligand L and a small quantity of MeCN [38, 39]. A third, rather promising route, which has not yet been applied for the preparation of the organotin-containing compounds, is the so-called 'thiosulfate-assisted' method that is carried out in aqueous solution [40]. This method consists of dissolving CuCN in $Na_2S_2O_3.5H_2O/H_2O$ solution. Then the ligand L is added and the mixture is heated and stirred until clear. The weak complex of $CuCN/S_2O_3^{2-}$ has a strong tendency to release CuCN to virtually any water soluble ligand to produce new $[(Cu)_n(CN)_m\cdot xL]$ complexes [41–43]. The fourth route depends on the use of the traditional high-temperature methods for preparing inorganic solid-state materials, which generally lead to isolation of thermodynamic phases. For instance, the hydrothermal chemistry of CuCN with bipodal organic ligands has been exploited to prepare a variety of homometallic 1D to 3D cyanide-bridged copper(I)-materials for which subtle changes in some of the already known factors often result in the formation of quite different structures [44–47]. In spite of the hydrothermal conditions that were exploited to minimize differential solubility and to affect crystallization [48], a mixture of products should be obtained in many cases. Also, owing to the complexity of the solvothermal reactions, in principle, the control and prediction of crystal structures would not be possible. On the other hand, the oxidation state of the metal could be affected by high temperature and pressure. However, reactions containing copper(I) exhibit thermodynamic stability with respect to Cu(II) species at such elevated temperatures and pressures [44]. Therefore, routes one and

two are suitable and promising for obtaining unique organotin or organotin-free compounds at room temperature.

The structure of **1** is quite different than **3.** The structure of **3** is composed of 1D-[Cu(CN)] chains penetrating 2D-$[Cu(CN)(pyz)]_n$ networks, which create sheets of fused [Cu6(CN)4(pyz)2] rings [37]. The interesting feature in this structure is the presence of the isolated –[Cu(CN)] chains. In the case of **1**, the pyz serves to link one chain to four neighboring chains thereby generating cyclic sub-structures of formula $[Cu_8(CN)_6(pyz)_2]$ and $[Cu_6(CN)_2(pyz)_4]$, which produces box-like structures. Because of the encompassing considerable volume within the box-like structure, equivalent frameworks are found to interpenetrate each other. On the other hand, the structure of **1** resembles **2** in the formation of cyclic rings and the equivalent interpenetrating networks in spite of the fact that they are different in ring size and the length of the spacer that contains the Me_3Sn fragment, Cu–CN–Me_3Sn–NC–Cu. The basic sub-units of **2** consist of distorted-adamandoid Cu_{10} cages whose surfaces are surrounded either by $[Cu_6(pyz)_4\{Sn\text{-}(NC)_2\}_2]$ or by $[Cu_6(pyz)_2\{Sn(NC)_2\}_4$ rings [36]. The structure of **1** could be also compared to [{Cu(l-CN)}$_2$(l-Me$_4$-pyz)-dioxane]n, **4** [18]. The structure of **4** propagates in the three-dimensions creating two types of cavities; a small rectangular cavity and a large hexagonal cavity forming two independent networks that are interpenetrating to form a two-fold interpenetrated structure. The rhomboidal cavities are filled by dioxane as guest molecule [18]. The steric hindrance of the methyl groups causes the formation of a twofold interpenetrated structure while in **1**, an inextricably interpenetration is observed.

Thus, the cyclic structures apparently reflect the connectivity as well as the linear disposition of pyz, its derivatives and the coordination preference of the Cu(I) sites. It is noteworthy that 2D materials exhibit networks threaded by $[Cu(CN)]_n$ chains, while the 3D structures are interpenetrating.

Finally, the luminescent solids have potential applications in molecular sensing systems since chemisorption of small molecules has been shown to alter the luminescence behaviour [35]. The red shift observed of the emission bands of **1** relative to that of CuCN is due to the coordination of pyz to the Cu(I) sites causing the bent structure of the CuCN chains.

4 Supplementary material

Crystallographic data for the structural analyses have been deposited with the Cambridge Crystallographic Data Center, CCDC, deposition No. CCDC 933949. These data can be obtained free of charge at www.ccdc.cam.ac.uk/conts/retrieving.html (or from the Cambridge crystallographic Data Center, 12 Union Road, Cambridge CB21EZ, UK; Fax: +44 1223/336 033; E-mail: deposit@ccdc.cam.ac.uk).

References

1. B.J. Hathaway, in Comprehensive Coordination Chemistry, vol. 5, ed. by G.Wilkinson (Pergamon, Oxford, 1987), p. 33
2. C. Janiak, Angew. Chem. Int. Edn Engl. **36**, 1431 (1997)
3. S.E.H. Etaiw, S.N. Abdou, J. Inorg. Organomet. Polym. **22**, 780 (2012)
4. S.E.H. Etaiw, S.A. Amer, M.M. El-bendary, J. Mater. Sci. **45**, 1307 (2010)
5. B.F. Hoskins, R. Robson, J. Am. Chem. Soc. **112**, 1846 (1990)
6. H. Yuge, T. Iwamoto, J. Inclusion Phenom. **26**, 119 (1996)
7. L.C. Brousseau, D. Williams, J. Kouvetakis, M. O'Keefe, J. Am. Chem. Soc. **119**, 6292 (1997)
8. W.P. Fehlhammer, M. Fritz, Chem. Rev. **93**, 1243 (1993)
9. R.G. El-sharkawy, A.S. Badr El-din, S.E.H. Etaiw, Spectrochim. Acta. Part A **79**, 1969 (2011)
10. S.E.H. Etaiw, S.A. Amer, M.M. El-Bendary, J. Inorg. Organomet. Polym. **21**, 662 (2011)
11. N.A. Khan, N. Baber, M.Z. Iqbal, M. Mazhar, Chem. Mater. **5**, 1283 (1993)
12. N. Krause, A. Gerold, Angew. Chem. Int. Ed. Engl. **36**, 186 (1997)
13. S.E.H. Etaiw, A.S. Sultan, A.S. Badr El-din, Eur. J. Med. Chem. **46**, 5370 (2011)
14. S.E.H. Etaiw, A.S. Sultan, M.M. El-bendary, J. Organomet. Chem. **696**, 1668 (2011)
15. A. Horváth, C.E. Wood, K.L. Stevenson, Inorg. Chem. **33**, 5351 (1994)
16. X. Liu, G.-C. Guo, A.-Q. Wu, L.-Z. Cai, J.-S. Huang, Inorg. Chem. **44**, 282 (2005)
17. X. Liu, G. –C. Guo. Cryst. Growth Des. **8**, 776 (2008)
18. S.E.H. Etaiw, A.S. Badr El-din, J. Inorg. Organomet. Polym. **21**, 110 (2011)
19. D.J. Chesnut, D.Plewak, J. Zubieta, J. Chem. Soc. Dalton Trans. 2567 (2001)
20. S.E.H. Etaiw, M.M. El-bendary, J. Inorg. Organomet. Polym. **20**, 739 (2010)
21. S.-W. Liang, M.-X. Li, M. Shao, Z.-X. Miao, Inorg. Chem. Comm. **9**, 1312 (2006)
22. S.E.H. Etaiw, T.A. Fayed, M.B. El-zaria, S.N. Abdou, J. Inorg. Organomet. Polym. **21**, 36 (2011)
23. S.E.H. Etaiw, T.A. Fayed, S.N. Abdou, J. Organomet. Chem. **695**, 1918 (2010)
24. A.F. Wells, Structural inorganic chemistry, 3rd edn. (Oxford U.P., London, 1962), pp. 487–490
25. W. Dannhauser, P.A. Vaughan, J. Am. Chem. Soc. **77**, 896 (1955)
26. N.P. Rath, E.M. Holt, J. Chem. Soc. Chem. Commun. 665 (1986)
27. P. Leoni, M. Pasquali, C.A. Ghilardi, J. Chem. Soc. Chem. Commun. 240 (1983)
28. M.J. Schilstra, P.J.M.L. Birket, G.C. Verschoor, J. Reedijk, Inorg. Chem. **21**, 2637 (1982)
29. S.A. Koch, R. Filkar, M. Miller, T.O. Sullivan, Inorg. Chem. **23**, 121 (1984)
30. A. Spalletti, G. Cruciani, U. Mazzucato, J. Mol. Str. **612**, 339 (2002)
31. H. H. Jaffe′, M. Orchin, Theory and Applications of Ultraviolet Spectroscopy, Fifth Printing (John Wily and Sons, Inc., 1970)
32. T.A. Tronic, K.E. de Krafft, M.J. Lim, A.N. Ley, R.D. Pike, Inorg. Chem. **46**, 8897 (2007)

33. M.J. Lim, C.A. Murray, T.A. Tronic, K.E. de Krafft, A.N. Ley, J.C. de Butts, R.D. Pike, H. Lu, H.H. Patterson, Inorg. Chem. **47**, 6931 (2008)
34. K.L. Stevenson, J.H. Jarboe, S.A. Langmeyer, T.W. Acra, Inorg. Chem. **42**, 3559 (2003)
35. C.A. Bayse, T.P. Brewster, R.D. Pike, Inorg. Chem. **48**, 174 (2009)
36. E. Siebel, A.M.A. Ibrahim, R.D. Fischer, Inorg. Chem. **38**, 2530 (1999)
37. D.J. Chesnut, D. Plewak, J. Zubieta, J. Chem. Soc., Dalton Trans. 2567 (2001)
38. R. Eckhardt, H. Hanika-Heidl, R.D. Fischer, Chem. Eur. J. **9**, 1795 (2003)
39. R. Eckhardt, R.D. Fischer, Inorg. Chem. Commun. **3**, 433 (2003)
40. F.B. Stocker, T.P. Staeva, C.M. Rienstra, D. Britton, Inorg. Chem. **38**, 984 (1999)
41. F.B. Stocker, M.A. Troester, Inorg. Chem. **35**, 3154 (1996)
42. F.B. Stocker, P. Fadden, S. Dreher, D. Britton, Inorg. Chem. **38**, 3251 (1999)
43. F.B. Stocker, M.A. Troester, D. Britton, J. Chem. Crystallogr. **30**, 389 (2000)
44. D. J. Chesnut, D. Plewak, J. Zubieta, J. Chem. Soc. Dalton Trans. 2567 (2001)
45. D.J. Chesnut, A. Kusnetzow, R.R. Birge, J. Zubieta, J. Chem. Soc. Dalton Trans. 2581 (2001)
46. D.J. Chesnut, A. Kusnetzow, R.R. Birge, J. Zubieta, Inorg. Chem. **38**, 5484 (1999)
47. D.J. Chesnut, D. Hagrman, P.J. Zapf, R.P. Hammond, R.J. LaDuca, R.C. Haushalter, J. Zubieta, J. Coord. Chem. Rev. **190**, 757 (1999)
48. D. Hagrman, J. Zubieta, J. Chem. Soc. Chem. Commun. 2005 (1998)